Title
Single molecule recordings of lysozyme activity

Journal
Physical Chemistry Chemical Physics, 15(36)

ISSN
0956-5000

Authors
Choi, Yongki
Weiss, Gregory A
Collins, Philip G

Publication Date
2013

DOI
10.1039/c3cp51356d

Peer reviewed

PCCP

Physical Chemistry Chemical Physics

www.rsc.org/pccp

Volume 15 | Number 36 | 28 September 2013 | Pages 14825–15244

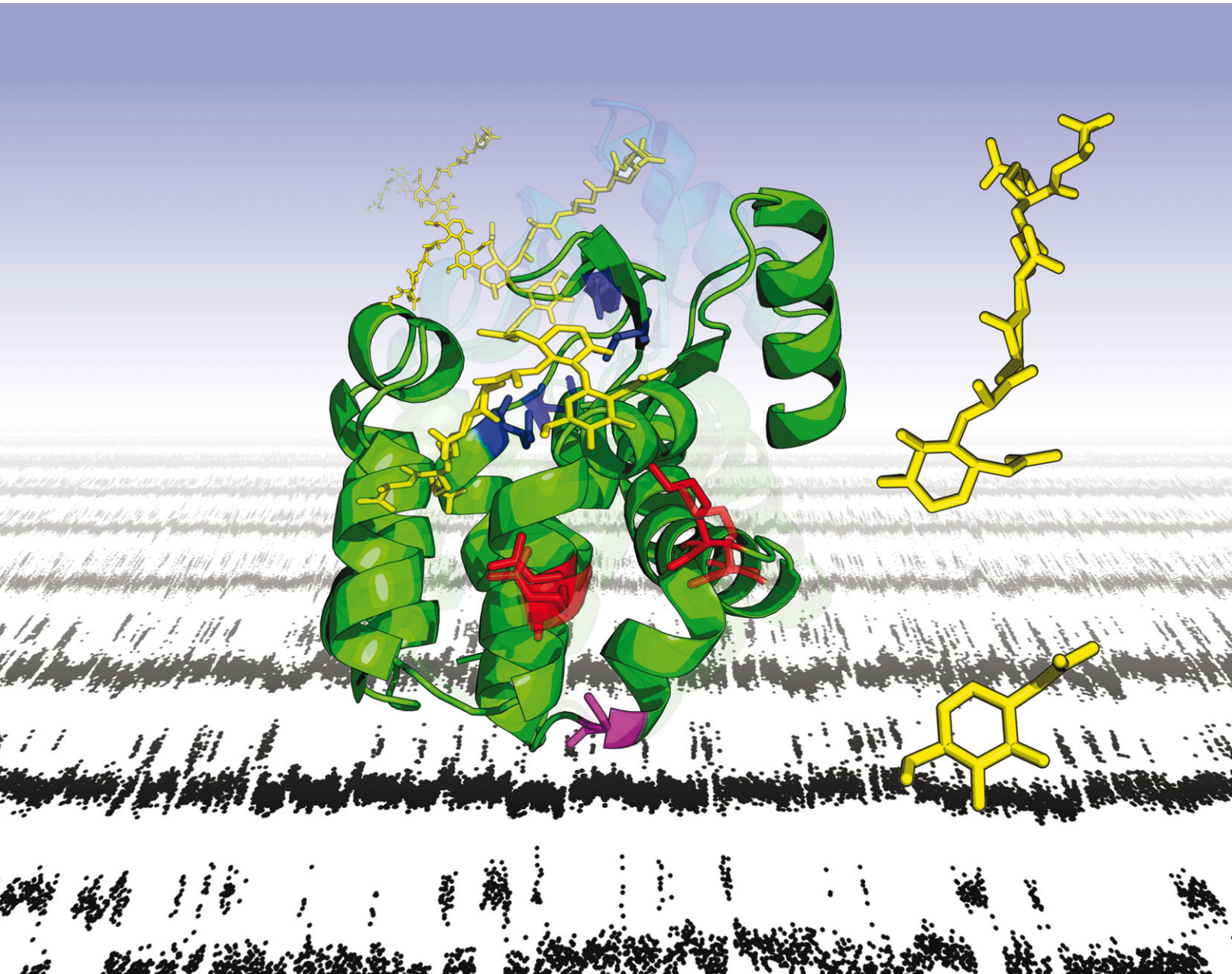

Includes a collection of articles on the theme of superresolution imaging and fabrication with light

ISSN 1463-9076

PERSPECTIVE
Collins *et al.*
Single molecule recordings of lysozyme activity

1463-9076(2013)15:36;1-J

PCCP

RSC Publishing

PERSPECTIVE

View Article Online
View Journal | View Issue

Single molecule recordings of lysozyme activity

Cite this: *Phys. Chem. Chem. Phys.*, 2013, **15**, 14879

Yongki Choi,[a] Gregory A. Weiss[b] and Philip G. Collins*[a]

Received 30th March 2013,
Accepted 31st May 2013

DOI: 10.1039/c3cp51356d

www.rsc.org/pccp

Single molecule bioelectronic circuits provide an opportunity to study chemical kinetics and kinetic variability with bond-by-bond resolution. To demonstrate this approach, we examined the catalytic activity of T4 lysozyme processing peptidoglycan substrates. Monitoring a single lysozyme molecule through changes in a circuit's conductance helped elucidate unexplored and previously invisible aspects of lysozyme's catalytic mechanism and demonstrated lysozyme to be a processive enzyme governed by 9 independent time constants. The variation of each time constant with pH or substrate crosslinking provided different insights into catalytic activity and dynamic disorder. Overall, ten lysozyme variants were synthesized and tested in single molecule circuits to dissect the transduction of chemical activity into electronic signals. Measurements show that a single amino acid with the appropriate properties is sufficient for good signal generation, proving that the single molecule circuit technique can be easily extended to other proteins.

Introduction

Traditional enzymology is primarily based on ensemble averages of enzyme populations. Over the past two decades, however, many techniques have been developed for monitoring chemical activity with single molecule precision. Single molecule studies offer new insights into molecular activity by resolving the timing and intermediate steps of catalytic cycles. In addition, single molecule resolution removes the averaging effects present in ensemble measurements to unravel the unique reaction trajectories of a particular molecule. These trajectories characterize the minute-by-minute changes in a molecule's kinetics through which activity depends upon conformational disorder, dynamics, and, in some cases, memory effects.

[a] *Department of Physics and Astronomy, University of California at Irvine, Irvine, California 92697, USA. E-mail: collinsp@uci.edu*
[b] *Departments of Chemistry and Molecular Biology and Biochemistry, University of California at Irvine, Irvine, California 92697, USA*

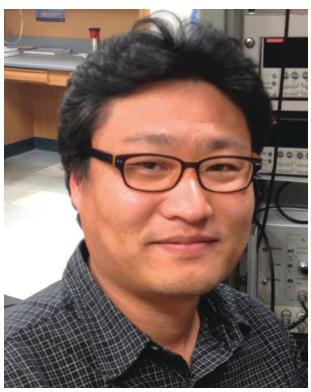

Yongki Choi

Yongki Choi is a postdoctoral researcher at University of California Irvine. He received his PhD in Physics from the City University of New York. His research has focused on the areas of bioelectronics, including biosensors and bio-fuel cells. At UCI, he has helped to develop new techniques for electronic biosensing with single molecule resolution to the been developing a new single-molecule technique with nanocircuits to investigate complex protein dynamics and functions of single molecules, including DNA polymerase and protein kinase A.

Gregory A. Weiss

Gregory Weiss earned undergraduate and graduate degrees from the University of California, Berkeley and Harvard University, respectively. Awarded a NIH Kirschstein NRSA from the NIH, he pursued post-doctoral studies at Genentech. In 2000, he joined the faculty at UC Irvine where his laboratory focuses on combinatorial biology, membrane proteins and bioelectronics. Tenured in 2006, he is currently a full Professor and Vice Chair in the Department of Chemistry. His awards include Outstanding Professor in the School of Physical Sciences at UC Irvine (elected by the graduating students), Beckman Foundation Young Investigator, and AAAS Fellow.

Two classes of techniques are currently in use in single molecule research. In the class of force-based techniques, a peptide,[1] DNA,[2,3] or other long-chain molecule[4] is anchored between two surfaces and stretched, sometimes with the additional influence of a processive enzyme.[5,6] For example, scanning probe techniques pull directly on molecules using a micromachined cantilever.[2] Optical and magnetic tweezers control the stretching force more indirectly, by anchoring the molecule to a moveable bead.[4,7,8]

Optical fluorescence is the foundation for a second class of single molecule techniques. Many biomolecules fluoresce weakly or not at all, which provides low background fluorescence for experiments with fluorophores conjugated to DNA, RNA and proteins. In fact, the technique of Förster resonance energy transfer (FRET), has become a standard tool for single molecule enzymology.[9–12] By attaching fluorophores to a specific sites in a protein structure, single molecule motions can be transduced into a color-coded blinking that can provide information about the distances between fluorophores.

Recently, we have demonstrated a third type of single molecule technique that is purely electronic.[13–17] By attaching single molecules to a sufficiently sensitive electronic circuit, we have recorded enzyme motions and catalytic activity as electrical signals rather than as pulses of light or modulations of force. The electrical signals encode specific protein motions with microsecond resolution over minutes and hours, providing very long duration recordings of single molecule dynamics. The stability and resolution dramatically improves upon force- and fluorescence-based techniques, making single molecule bioelectronics an exciting addition to the scientific toolbox. In addition, single molecule bioelectronic devices can potentially take advantage of the wide-ranging capabilities of solid state electronics, and could lead to a powerful platform of fully integrated, hand-held diagnostic devices.

This paper reviews the study of bacteriophage T4 lysozyme accomplished using the single molecule bioelectronic technique.[13–15] After a brief introduction to lysozyme's properties, the paper describes the device fabrication and principles of its operation. The majority of the paper focuses on the analysis of continuous electronic recordings containing many thousands of chemical events. These recordings provided a complete picture of lysozyme's complex activity, including memory effects, dynamic disorder, and processive variability, all of which were inaccessible to ensemble measurements. The final section concludes with a description of the operative signal transduction mechanisms, providing guidelines for the measurement of equally rich data sets from other biomolecules of interest.

Philip G. Collins

Philip Collins received BS degrees in Physics and Electrical Engineering at the Massachusetts Institute of Technology, and a PhD in Physics from the University of California, Berkeley. He worked at IBM's T. J. Watson Research Center and at Nanomix, a nanotechnology startup company, before joining the Department of Physics and Astronomy at UC Irvine in 2002. His expertise is in the electronic properties of nanoscale materials, particularly carbon nanotubes, and his research group establishes methods of building circuits at the molecular scale. He has been awarded an NSF CAREER research award and multiple campus-wide teaching awards.

Lysozyme and single-molecule lysozyme studies

The enzyme lysozyme is found in tears, saliva, and other mucus secretions. It selectively catalyzes the hydrolysis of the β-1,4 glycosidic bond between *N*-acetylmuramic acid (NAM) and *N*-acetyl-D-glucosamine (NAG) in peptidoglycans, the polysaccharides that compose the cell walls of gram-positive bacteria.[18] By attacking these bonds, lysozyme plays an important role in the innate immune system. In addition, lysozyme orthologs have important roles in bacteriophage lifecycles, allowing the virus to enter and exit the bacterial cell.

Lysozyme is an excellent model system for calibrating a new single-molecule technique because past research has already uncovered a great deal about its structure and activity.[19–23] Two lysozyme subdomains surround a deep cleft in which the peptidoglycan substrate binds. In T4 lysozyme, a hinge-like, mechanical closing of the subdomains helps distort and strain the NAM ring of the glycan substrate; then, lysozyme residues E11, E20 and T26 can interact with the substrate, and complete the hydrolysis of an NAG–NAM glycosidic bond.[24,25] While this mechanism of catalysis is well understood, whether lysozyme is a processive enzyme remains a longstanding question. Lysozyme could either sequentially attack each glycosidic bond along the peptidoglycan strand for a processive mechanism, or release the substrate after each hydrolysis in a distributive mechanism of catalysis. Fig. 1 depicts the domain structure for the T4 lysozyme used in this work, with important catalytic residues E11 and T26 highlighted in blue.

Lysozyme's mechanical hinge motion of 0.8 nm is ideal for precise, single molecule FRET (smFRET) studies,[24] and careful measurements have observed a range of interesting behaviors. For example, hinge motion can occur at two different rates, only one of which is effective for catalysis.[26] When the hinge opens and closes at rates of 10–80 s^{-1}, glycosidic bonds are being broken. Faster motions in a separate and distinct range of 200–400 s^{-1} are nonproductive; these fast dynamics do not result in glycosidic bond hydrolysis, even though peptidoglycan may be bound within the cleft during their motions. A single lysozyme molecule can remain in one state or the other over long durations, indicating a ''static disorder'' between at least two stable conformations. Unfortunately, smFRET methods are poor at performing long-duration measurements that can probe the stability of static disorder, since fluorophores themselves

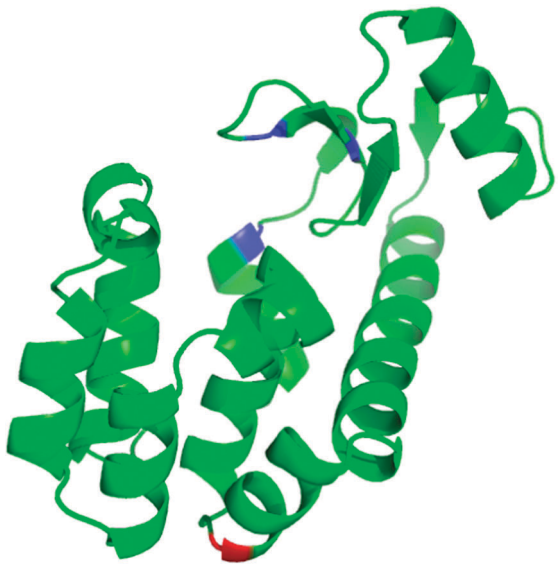

Fig. 1 Bacteriophage T4 lysozyme (PDB: 6LZM). The single-cysteine lysozyme variant used in these electronic studies encodes a S90C mutation (red) that serves as the point of attachment to the SWNT FET. Key catalytic residues surrounding the active site are highlighted in blue.

blink and quench over time scales of 1–10 s. Nevertheless, static disorder, along with fast- and slow-scale dynamic disorder described as "bunching" and "memory," respectively, have made lysozyme a rewarding system that continues to stimulate research.[27]

For our experiments, open reading frames encoding T4 lysozyme variants were synthesized by splice overlap extension PCR based upon a pseudo-wild-type variant with the substitutions C54T and C97A (a generous gift from Prof. Brian Matthews, University of Oregon).[28,29] Amplicons encoding each of the variants were subcloned into the pET28 vector for protein overexpression in *E. coli*. Following expression, lysozyme was isolated and purified by centrifugation, cation exchange, and size-exclusion chromatography. The homogeneity of the final lysozyme solutions was >95%, as estimated by SDS PAGE. Synthesis protocols were described in greater detail in ref. 14.

Peptidoglycan isolated from *Micrococcus luteus* was purchased from Sigma-Aldrich and used as a substrate to assay lysozyme activity.[30] The substrate was suspended to a final concentration of 25 μg ml^{-1} in PBS at pH 7.5. This concentration insures the presence of excess substrate for V_{max} conditions. After preparation, the peptidoglycan suspension was allowed to settle before use. Typically, 250 μL of the supernatant solution was pipetted for application to the bioelectronic devices. This technique excluded the largest peptidoglycan fragments and aggregates. Additional data acquired using decreased substrate concentrations of 5 and 1 μg ml^{-1} were not detectably different from the results presented here.

Electronic devices for single molecule recording

The general principle of building single biomolecule circuits has been motivated by the complex kinetics of molecules like lysozyme and the need for longer duration monitoring. This goal is a repurposing of "molecular electronics," which in the past has been solely motivated by extending the scaling trends of traditional, digital microelectronics.[31–33] Rather than imagining biomolecules as miniature memory elements or silicon replacements, we argue that the positive impact of building single biomolecule devices could be in revealing the dynamic chemistry of complex molecules. The devices could provide an opportunity to interface solid-state electronics with biochemical activity, in order to watch and analyze the dynamic signals generated as target molecules arrive, activate, or bind to a target.[34]

Most molecular electronic architectures investigated in the past have been unsuitable for this goal. Mechanical break junctions[35–39] and electromigrated gaps[40–43] have lacked the sensitivity, bandwidth, or mechanical stability to record ongoing single molecule dynamics. More traditional architectures like field effect transistors (FETs) provide high bandwidth and mechanical stability, but typically are fabricated at much larger scales. Research efforts have pursued the limits of FET size and sensitivity using traditional silicon as well as more novel nanomaterials. Low dimensional channel materials such as single-walled carbon nanotubes (SWNTs),[44–49] silicon nanowires,[50–55] nanoclusters,[56,57] and graphene[58,59] have all been investigated as exposed, environmentally sensitive FETs.

Ultimately, SWNT FETs[60–62] have an unmatched sensitivity that originates from their quasi one-dimensional electronic structure and low carrier concentration. In a pristine SWNT, charge carriers scatter very infrequently (the inelastic mean free path approaches 1 μm at room temperature), so SWNT resistance can be a sensitive indicator of additional environmental interactions. The one-dimensionality of SWNTs further means that carriers cannot simply redistribute around a scattering site, as they do in metal films or even atomically-thin graphene. In a one-dimensional wire, every individual electron that contributes to an electrical current directly interacts with a scattering site.

Taking advantage of these properties requires fabricating SWNT devices and then tailoring the scattering site to contain the biomolecule of interest. Fortunately, many research groups have contributed innovations that today make SWNT device fabrication straightforward. Our research has used catalyst-assisted chemical vapor deposition to synthesize isolated SWNTs in controlled locations on electronic substrates like Si wafers. Our typical conditions, described in detail in previous publications,[14] resulted in a dilute areal density of approximately 0.01 SWNTs per μm^2 across a 4″ wafer surface, with SWNT diameters in the range of 1.1–1.6 nm and lengths of 10–100 μm. On top of these SWNTs, photolithography patterned an array of source and drain electrodes contacting individual SWNTs. Contacting metals have included Pt, Au, Pd, or Ti, without noticeable differences in single-molecule transduction. After lithography, individual source–drain electrode pairs were electrically probed to identify SWNT connections. Topographic imaging by non-contact atomic force microscopy (AFM) ensured that each device comprised only one SWNT and confirmed that the SWNT was free of particulates.

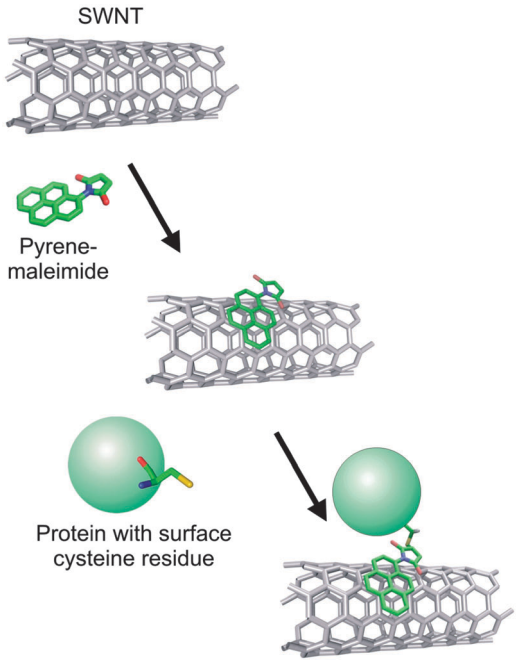

Fig. 2 Biofunctionalization scheme. The bare SWNT is biofunctionalized in two steps. First, noncovalent π–π stacking adheres pyrene-maleimide linkers in the desired density. Second, covalent thioether bonds are formed between the maleimide and the free cysteine engineered into the surface of lysozyme.

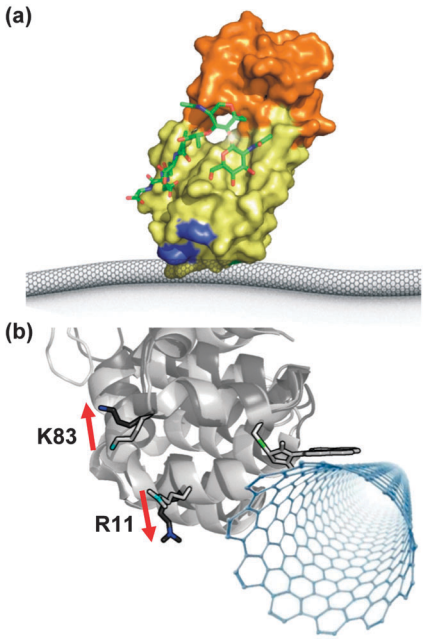

Fig. 3 Likely attachment orientation of lysozyme. (a) Lysozyme attached to a SWNT with peptidoglycan shown bound in the active site. Coloring distinguishes the upper and lower domains and residues K83 and R119. (b) Closeup of the pyrene-maleimide linkage, with open and closed lysozyme crystal structures shown in light and dark grey. The movements of K83 and R119 during the enzyme open to closed conformational change are highlighted with arrows.

Following synthesis and initial characterization, SWNTs were dilutely biofunctionalized. Many researchers have investigated SWNTs coated with biomolecules or other sensitizing materials, and we have simply leveraged SWNT sensitivity by tailoring such coatings to the dilute limit of one individual molecular attachment. In fact, we have developed both covalent[63–68] and non-covalent[13,14] schemes for building single molecule devices.

The work with lysozyme was accomplished with a particular, two-step noncovalent scheme outlined in Fig. 2. First, devices were soaked in a solution of pyrene-maleimide (1 mM *N*-(1-pyrenyl)maleimide in ethanol) that served as bifunctional linker molecules. The pyrene groups adhered to the SWNT sidewalls through strong π–π interactions,[46,69] but could be diluted with repeated rinsing (0.1% Tween-20 in ethanol). In a second step, the devices were incubated in a solution of pseudo-wild-type, single-cysteine variant of T4 lysozyme (C54T, C97A, and S90C, hereafter referred to simply as "lysozyme").[28,70] The mutagenic modifications were designed to leave a single exposed cysteine on the protein's surface for attachment to the linker. Through nucleophilic Michael addition, the C90 cysteine formed stable thioether bonds with maleimides adhered to the SWNT.[71] Limiting the lysozyme to have only one cysteine meant that the molecule would attach to the SWNT device in a predictable orientation.

Fig. 3a depicts the orientation of lysozyme attached to a SWNT. The two subdomains are colored yellow and orange and a peptidoglycan fragment is shown bound in the active site. The active site is located 3.1 nm from the C90 attachment site, so that peptidoglycan can freely access it from solution. Fig. 3b is a higher magnification model of the C90 linkage region, which is partially hidden in Fig. 3a. Although peptidoglycan binding occurs far from the linkage, the interaction with the substrate drives allosteric motions of the entire enzyme. In Fig. 3b, open and closed conformations of lysozyme are overlaid in light and dark grey, respectively, to suggest motions of the enzyme in the immediate vicinity of the SWNT.

The successful production of devices with single lysozyme molecules proved to be remarkably straightforward, aided by a combination of effects. First, the active area of a SWNT FET began at an extremely small scale of only 1000–4000 nm^2. Second, this target area was further reduced by controlling the surface density of pyrene-maleimide linkers. The number of potential attachment sites on a SWNT FET was easily tailored by varying solution concentrations and rinsing protocols. Third, the Michael addition reaction can be a relatively inefficient reaction, and only a small number of the available maleimides successfully reacted with a protein. On average, attachment densities of 1 molecule per μm of SWNT length were typical. After developing the initial procedure, hundreds of devices have been fabricated and tested using >10 different lysozyme variants. In addition, the single-cysteine design has now been reproduced with two additional enzymes,[16,17] indicating that the success was not unique to the properties of lysozyme.

Once the average attachment yield had been determined using long SWNTs or large-area devices, a device design could be finalized. In our experience, it has proven useful to coat most of the SWNT device with a passivating layer of either

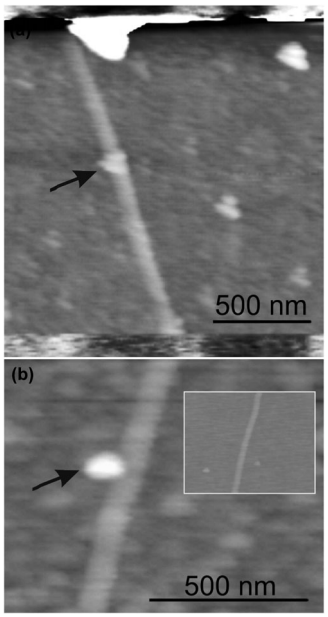

Fig. 4 AFM topography of single molecule devices. (a) A typical device with a single lysozyme attachment (arrow). The SWNT extends under the protective PMMA coating (top and bottom) to connect with metal electrodes. (b) A similar device at higher magnification. The AFM lateral resolution is tip limited, but the height measurements are reliable. (inset) The same SWNT before biofunctionalization.

alumina or polymer to reduce noise, protect the contact electrodes, and limit nonspecific adsorption events. We have used a second lithographic step to expose short segments of SWNT (0.2 to 1.0 μm) to the environment, leaving the rest of the device protected. Successful single molecule biofunctionalization of different exposed lengths has been easily accommodated by varying the protein concentration and incubation time.

Fig. 4 depicts example topographic images of the resulting devices. AFM imaging was generally performed in liquid unless all electronic measurements were complete, in which case the device could be rinsed off, dried, and measured in air. With care and diligent rinsing, surfaces were kept clean enough to easily resolve 1 nm SWNTs and single attached proteins (arrows). Like most proteins, lysozyme was many times larger than a SWNT diameter. When measured in air, the apparent height of lysozyme attachments was typically 5 to 7 nm.

After confirming an attachment to a SWNT device, the measurement protocol consisted of recording electrical signals from the device. We generally measured fluctuations in the current $I(t)$ flowing through a SWNT under constant bias conditions. A constant source–drain bias of 50 to 100 mV was sufficient to drive currents of 1 to 100 nA through the SWNT, as measured by a current preamplifier attached at either electrode. The amplified $I(t)$ signal was digitized, displayed to the user, and stored for later analysis. Continuous measurement for at least 600 s provided long recordings suitable for generating good statistics of individual events. Typical bandwidths of 20 to 50 kHz provided temporal resolutions down to 20 μs, using only commercial instruments and without any device optimization. For comparison, fluorescence shot noise typically limits FRET to temporal resolutions of 100 μs up to 1 ms.[72]

$I(t)$ reports the electrical resistance of the SWNT, which in the simplest electrical model is a series combination of contact effects, intrinsic resistivity, and any additional scattering caused by the protein attachment. Fortunately, a substantial portion of the total resistance can be caused by the attachment, since the SWNT is otherwise a high conductivity conductor.[44,73,74] This co-location of attachment, resistance, and SWNT sensitivity is one key to successful signal generation. The lysozyme attachment induces a dynamic, time varying resistance in the SWNT that is sensitive to the presence of substrate in the surrounding electrolyte. To focus on these fluctuations, analysis begins by removing the DC component from $I(t)$ using a 1 or 10 Hz highpass filter. The resulting fluctuations $\Delta I(t)$ have a mean value of zero that may be analyzed using any of the techniques common to the single molecule and single ion channel research communities, such as the software package vbFRET.

The electrical measurements were performed with the active portion of the SWNT device submerged in electrolyte. For lysozyme measurements, we used phosphate-buffered saline (PBS; 138 mM NaCl, 2.7 mM KCl, 8.1 mM Na_2HPO_4, 1.5 mM KH_2PO_4, pH 7.5). The electrolyte was applied to the active region using either a pipette or microfluidics and controlled electrochemically by a Pt pseudo-reference electrode. Holding the electrochemical potential constant with a low-noise source was important for stable and reproducible measurements. While grounding the electrolyte was a simple method of pinning its potential, it proved necessary to control at other voltages in the range of −0.4 to +0.2 V, depending on the particular sensitivity of the SWNT. An electrochemical bipotentiostat was helpful for measuring the SWNT's characteristics and selecting the most appropriate electrolyte bias.

Electronic measurements of lysozyme activity and processivity

With functionalization limited to one molecule, each SWNT device served as a high bandwidth sensor for monitoring single-molecule dynamics, providing access to real-time, dynamic transduction.

Fig. 5 shows the three primary categories of $\Delta I(t)$ signals that composed the lysozyme recordings. When peptidoglycan was absent, $\Delta I(t)$ exhibited an envelope of background noise that was typical for SWNT devices.[75,76] Upon adding peptidoglycan, we observed this same background noise during only 5% of the recordings (Fig. 5a). The remaining 95% of the recordings were filled with two-level fluctuations depicted in Fig. 5b and c. When peptidoglycan was removed from the measurement solution, these two-level fluctuation ceased and $I(t)$ returned to its baseline value. Therefore, we concluded that the baseline in Fig. 5a was associated with lysozyme's open conformation. Additional control experiments included devices fabricated with two different types of catalytically inactive variants having

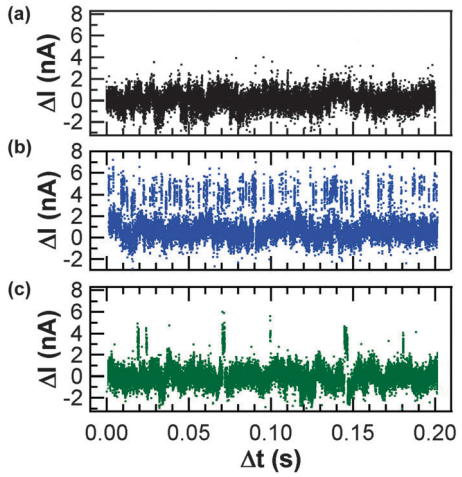

Fig. 5 Example electrical signals generated by single lysozyme molecules. (a) Baseline of SWNT FET in the absence of lysozyme activity. (b) Fast two-level fluctuations at rates of 200 to 300 s^{-1}. (c) Slow two-level fluctuations at rates of 10 to 70 s^{-1}.

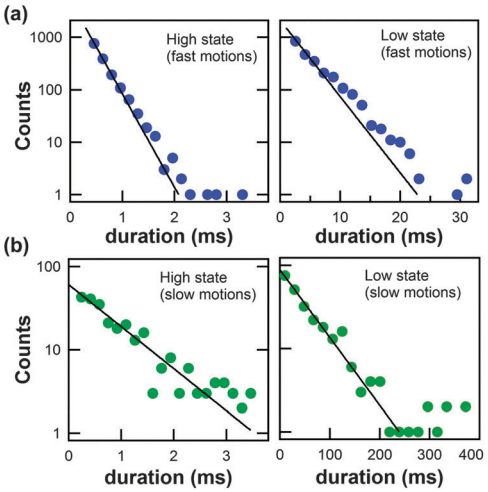

Fig. 6 Event distributions separated by type of motion. (a) During fast, non-productive closures, the high-current excursions last up to 3 ms. Low-current intervals have durations up to 30 ms. Solid lines depict single-exponential fits. (b) Distributions of high- and low-current events during slow motions, depicting the longer time scales for both.

the substitutions T26E and E11H. The E11H variant is unable to catalyze hydrolysis of the peptidoglycan substrate, whereas the T26E variant binds the peptidoglycan covalently and irreversibly.[77] None of the devices fabricated with these inactive variants produced two-level $\Delta I(t)$ fluctuations.

These control measurements indicated that two-level $\Delta I(t)$ fluctuations shown in Fig. 5b and c corresponded to the activity of the enzyme and that the high $I(t)$ value corresponded to lysozyme's closed conformation. With the active variants, two different rates of activity were observed, in agreement with smFRET measurements.[26] Nearly 50% of the recordings were filled with very rapid oscillations (Fig. 5b). Lysozyme remained in its open conformation for a few ms, on average, punctuated by brief excursions $\Delta I(t)$ lasting for about 0.25 ms. In the other half of the recordings, the oscillations occurred almost 20 times slower (Fig. 5c), with lysozyme remaining in its open conformation for 60 ms, on average.

Because the recordings extended for hundreds of seconds on any given molecule, excellent statistics could be generated for the different categories of lysozyme motion. Fig. 6 provides probability distributions for the durations of fast and slow oscillations, color-coded to match Fig. 5. All four distributions exhibited simple, Poisson statistics that fit single exponential time constants. For all four τ variables, Table 1 summarizes the mean values $\langle\tau\rangle$, standard deviations σ, and the mean-normalized statistical variances $r = \sigma^2/\langle\tau\rangle^2$. In addition, we calculated mean rates $k = (\langle\tau_{lo}\rangle + \langle\tau_{hi}\rangle)^{-1}$. For the faster two-level switching (blue), the instantaneous rate k_{fast} varied between 200 and 400 s^{-1} with a mean value k_{fast} = 316 s^{-1}. The slower fluctuations (green) had rates of 15 to 60 s^{-1} with a mean value k_{slow} = 15.4 s^{-1}. Both ranges are in excellent agreement with motions observed by smFRET. Using fluorescent substrates, smFRET had previously shown that lysozyme's slower motions correspond to peptidoglycan hydrolysis, whereas the faster motions are nonproductive conformational changes.[26,27,77]

The magnitude of one excursion, from a high $I(t)$ value to a low one or *vice versa*, was identical for the fast and slow oscillations. This constant magnitude suggested that the extent of lysozyme's hinge motion was nearly the same and independent of the rate of its motion. Similar conclusions have been drawn from smFRET measurements.[26,27,77]

A unique aspect of the electronic measurements was that a molecule's reaction trajectory could be followed indefinitely. Monitoring a single molecule for 600 s allowed us to directly observe interconversions between the catalytic (slow) and non-productive (fast) activities. On average, a molecule would spend 7 to 10 seconds at one rate before abruptly transitioning to the other. No particular transition region or other unusual activity was resolved during these changes.

This type of long-duration memory effect is very difficult to characterize in smFRET due to the limitations of fluorophore bleaching. Each of our recordings, on the other hand, included dozens of such transitions. We assigned each period of fast or slow activity a duration τ_{mem} and then calculated an average $\langle\tau_{mem}\rangle$ and standard deviation from the many independent sequences found in long recordings (Table 1). In general, effective catalytic processing continued for $\langle\tau_{mem}\rangle$ = 8.0 ± 3.0 s, and then was interrupted by equally-long periods of nonproductive motions.

Overall, nine independent times governing lysozyme's activities were directly measured from a single molecule. For the fast, nonproductive state, these included $\langle\tau_{lo}\rangle$, $\langle\tau_{hi}\rangle$, $\langle\tau_{mem}\rangle$, and the total proportion of time spent undergoing nonproductive motions. The same parameters were measured for the slow, catalytic processing state, and a $\langle\tau_{mem}\rangle$ value was measured for the inactive state. This level of detail was uniquely enabled by the long-term stability of the electronic monitoring technique.

Device stability also allowed measurements of the same enzyme under varying conditions. Measurements were performed at pH 5,

Table 1 Single molecule kinetic parameters for lysozyme processing peptidoglycan substrate

Parameter	pH 5	pH 7	pH 11
Catalytic processing (slow rate)			
$\langle\tau_{closed}\rangle$ (ms)	0.76 ± 0.05	0.95 ± 0.08	0.78 ± 0.09
r_{closed}	0.68 ± 0.15	0.74 ± 0.12	0.60 ± 0.15
$\langle\tau_{open}\rangle$ (ms)	87 ± 3.0	64 ± 2.0	86 ± 3.0
r_{open}	1.00 ± 0.18	1.06 ± 0.15	1.11 ± 0.23
ΔE (kcal mol^{-1})	2.84	2.53	2.82
k_{slow} (s^{-1})	11.4	15.4	11.5
$\langle\tau_{mem}\rangle$ (s)	9.3 ± 5.1	8.0 ± 3.0	12.0 ± 4.4
% time in state	16.3	41.1	21.1
Time-averaged catalytic rate (s^{-1})	1.8	6.3	2.4
Nonproductive binding (fast rate)			
$\langle\tau_{closed}\rangle$ (ms)	0.25 ± 0.01	0.26 ± 0.01	0.36 ± 0.01
r_{closed}	0.48 ± 0.10	0.43 ± 0.06	0.61 ± 0.08
$\langle\tau_{open}\rangle$ (ms)	4.80 ± 0.35	2.90 ± 0.10	3.90 ± 0.17
r_{open}	0.97 ± 0.13	0.99 ± 0.09	1.00 ± 0.10
ΔE (kcal mol^{-1})	1.77	1.45	1.43
k_{fast} (s^{-1})	198	316	235
$\langle\tau_{mem}\rangle$ (s)	6.2 ± 4.0	7.9 ± 2.3	5.4 ± 1.8
% time in state	72.4	52.1	63.8
Inactive			
$\langle\tau_{mem}\rangle$ (s)	0.83 ± 0.63	0.72 ± 0.25	0.96 ± 0.53
% time in state	11.3	6.8	15.0

7, and 11 on the same molecule to investigate how each of the 9 time constants varied with pH. Table 1 summarizes these results. Away from pH 7, the catalytic rate k_{slow} slowed down modestly (~25%) but $\langle\tau_{mem}\rangle$ increased by a similar fraction, so that the total number of chemical events in a processing sequence was nearly unchanged. However, catalytic activity was interrupted more frequently by longer and longer inactive periods at pH 5 and 11. Consequently, the time-averaged catalytic activity decreased 60 to 70% at these pH values, even though the instantaneous rate of lysozyme's opening and closing was little changed. Fig. 7 graphically depicts how the increasing durations of nonproductive and inactive motions reduced average catalytic activity.

Thermodynamically, the ratio of $\langle\tau_{hi}\rangle$ to $\langle\tau_{lo}\rangle$ defines an effective energy difference for any two-level system. In lysozyme, the closed state is much briefer than the open state, indicating that this conformation requires higher energy to access. Using Boltzmann statistics, this energy difference may be calculated as $\Delta E = k_B T \ln(\langle\tau_{hi}\rangle/\langle\tau_{lo}\rangle)$. During the fast, nonproductive motions, ΔE was approximately 1.4 kcal mol^{-1}, but during the slower, catalytic motions ΔE was nearly 2.5 kcal mol^{-1}. During the higher-energy, catalytically-effective closures, lysozyme mechanically distorts the NAM ring from a "chair" to a "skew boat" configuration. In this state, its glycosidic bond is more susceptible to hydrolysis. Taking lysozyme's opening and closing motions to be otherwise indifferent to whether chemistry occurs, the increase of 1.1 kcal mol^{-1} between nonproductive and catalytic motions can probably be interpreted as the extra energy required for this ring distortion and bond hydrolysis. Note, however, that these ΔE values specifically refer to measurements in which peptidoglycan is bound in the active site. When peptidoglycan is absent, neither our electronic data nor smFRET measurements observe lysozyme accessing its closed conformation. This lack of closures indicates that the closed conformation is inaccessibly higher in energy when substrate is absent.

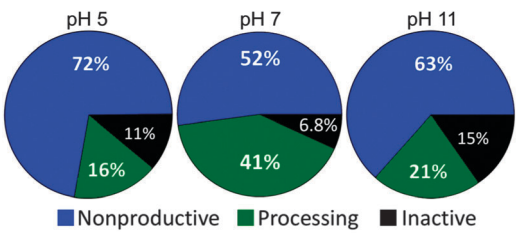

Fig. 7 pH dependence of lysozyme activity. The proportion of time spent in the nonproductive, catalytic processing, and inactive states varies with pH, with the highest catalytic activity at pH 7. Changes within each category are primarily caused by increases and decreases $\langle\tau_{mem}\rangle$, rather than from any effects on the instantaneous τ_{open} or τ_{closed} durations.

Many SWNT devices were fabricated and successfully measured, and not every lysozyme molecule exhibited identical rates. Fig. 8 shows that the different molecules had k_{slow} rates ranging from 15 to 65 s^{-1}, with an average $\langle k_{slow}\rangle$ = 30 s^{-1}. Not shown in Fig. 8 is the distribution for k_{fast}, which varied from 120 to 600 s^{-1} with a mean $\langle k_{fast}\rangle$ = 280 s^{-1}. The mean values are in good agreement with bulk activity measurements if the $\langle\tau_{mem}\rangle$ values described above are also considered. Individual molecules measured on different days tended to produce the same τ distributions, leading to the conclusion that molecule-to-molecule variation in Fig. 8 resulted from a type of static disorder that did not vary on the time-scale of days. The perturbing influence of the SWNT and nearby SiO_2 surface must certainly be considered as a potential source of such disorder, but it is also possible that conformational disorder played a role. Either way, this static disorder meant that even

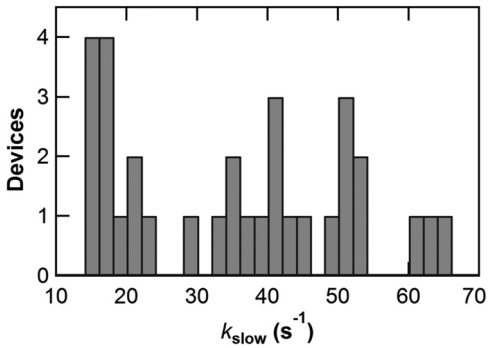

Fig. 8 Histogram of catalytic rates. Each single molecule device exhibited a different k_{slow}, suggesting molecule-to-molecule static disorder.

our longest measurements did not fully test the ergodic hypothesis. Future experiments in this direction would need to more widely vary the conformational energy landscape for a particular molecule, perhaps by denaturing and then refolding it between multiple measurements.

Most of the discussion above has focused on average values derived from the τ distributions, but one of the unique strengths of single-molecule studies is to look at event-to-event variability. By measuring thousands of independent events, we were able to calculate normalized variances r with small error bars. As shown in Table 1, r_{open} was calculated to be 1.06 ± 0.15, whereas r_{closed} was only 0.74 ± 0.12 during catalytic processing and even smaller, at 0.43 ± 0.06, during nonproductive motions. Analysis of distributions at three pH values showed that the r values did not depend on pH.

The first case is the simplest to interpret, because $r_{open} = 1$ indicates a reaction with only one rate-limiting step (*i.e.*, $\langle\tau\rangle = \sigma$ for a simple Poisson process).[78–80] Two or more rate-limiting steps are required to produce variances less than one, like those observed for r_{closed}.[78–80] Mathematically, two Poisson processes with equal rates cause $r = 0.5$, but the more common case of unequal rates leads to $0.5 < r < 1$. Three rate-limiting processes (or more) are necessary to produce $r < 0.5$. Therefore, the measurements definitively show that the closed state involves at least two and possibly three rate-limiting steps. While it might seem obvious to assign the catalytic hydrolysis to one of these steps, r_{closed} was smallest for the rapid motions corresponding to nonproductive binding. This finding indicated that lysozyme's fast, nonproductive closures were more complicated mechanistically than the slower, catalytically productive ones. The possibility of such complexity within a chemically inactive motion had not previously been appreciated.

In fact, the complexity of lysozyme's closure during nonproductive processing led us to question what remaining factors could be responsible. Ultimately, interpretation of the single molecule data was limited by the heterogeneous nature of the peptidoglycan. Peptidoglycan isolated from *Micrococcus luteus* is a diverse and extensively cross-linked mixture of peptidoglycan polysaccharide chains. Developing a mechanistic understanding of lysozyme's nonproductive motions required a simpler substrate.

In a collaboration with Muroplex Therapeutics, a synthetic peptidoglycan was synthesized with no cross-links.[13,81] Enzyme-assisted polymerization of a peptidoglycan precursor produced a linear substrate upon which lysozyme seemed to function normally in ensemble assays. The linear substrate still had structural diversity, because it ranged in length from 75 to 375 kDa. However, this synthetic substrate lacked the pentapeptide cross-links that convert peptidoglycan into an effective 2-dimensional structural material for bacterial cell walls.

Single molecule lysozyme devices were recorded variously processing the linear and cross-linked substrates, with extensive rinsing in between to eliminate cross contamination. The three types of activity described for Fig. 5 were observed using both substrates, but the proportion of time spent in fast, nonproductive motions was reduced by over 80% when lysozyme processed the linear substrate. Fig. 9 depicts this result using 3 minute I(t) records, color-coded using the previous scheme to depict slow, fast, and inactive periods. While individual events are not resolved at this low magnification, the long scale provides an immediate, visible comparison of $\langle\tau_{mem}\rangle$ for the three states and the interconversion between them. With the linear substrate, the periods of slow, catalytic processing (green) become longer, and the fast, nonproductive motions (blue) become shorter and less frequent. The amount of time in the inactive state (black) is nearly unchanged. Fig. 9c depicts the total percentage of time spent in each of the three states, with the nonproductive time dropping from 43% to only 7% of the time record for the synthetic linear substrate.

Because of this dramatic shift, we hypothesize that lysozyme's nonproductive motions are primarily associated with the cross-links in natural peptidoglycan. Without cross-links, catalytically effective motions were sustained for as long as 20 and 30 s. When cross-links were encountered, this activity was interrupted and lysozyme adopted its faster rate motion. Inactive segments (black) were not observed at any of the fast–slow or slow–fast transitions, indicating that substrate dissociation was not occurring. In fact, the recordings showed continuous catalytic processing before and after every nonproductive (blue) segment. This observation indicated that lysozyme was able to effectively get around cross-links without substrate dissociation, for example by transiting from one strand to another. Lysozyme cannot hydrolyze the cross-links themselves, but it appears to have evolved a particular type of motion that enables such transits. In this interpretation, the value of $\langle\tau_{mem}\rangle$ for the fast, nonproductive motions represents the mean time for a transit to be successful.

Besides its effects on the nonproductive motions, the presence of cross-links also introduces a unique type of inactive state. In Fig. 9a and b, inactive states are color-coded black when the enzyme activity paused in the open conformation, but yellow when the enzyme activity paused with the enzyme in its closed conformation. No yellow-coded data are present in Fig. 9b, indicating that lysozyme never became ''stuck'' in its closed state when processing linear substrate. Lysozyme only became inactive in its closed conformation in the presence of cross-links, and moreover these periods only occurred if

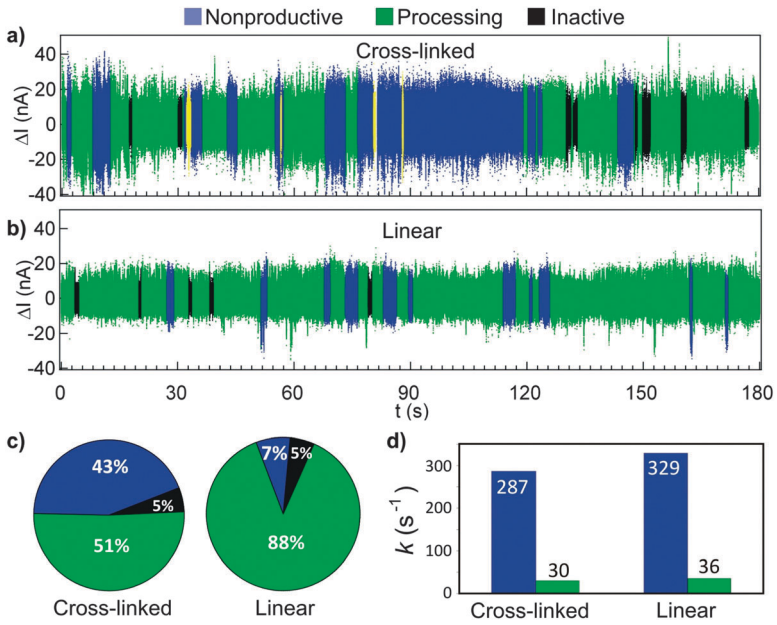

Fig. 9 Processive comparison of linear and cross-linked substrate. (a) Lysozyme processing of cross-linked peptidoglycan results in nearly equal periods of fast nonproductive motions (blue) and slow catalytic motions (green). (b) Processing of synthetic, linear substrate is substantially biased toward catalytic motions. (c) Percentage of time spent in each mode of activity for the two types of substrates. Note that the percentage of time spent inactive is independent of the substrate. (d) Average instantaneous rates k_{fast} and k_{slow} for both substrates. The presence of cross-links decreases the turnover rate for both types of motion.

bracketed by nonproductive motions. Therefore, the behavior of becoming "stuck" closed is unique to the faster motions that lysozyme adopts when attempting to transit cross-links. We note that both linear and cross-linked substrates exhibited equal fractions of the inactive, open configuration (black), which most likely occurred upon substrate dissociation. This distinction between inactive-open and inactive-closed states was not made in Fig. 5 or Table 1 because the existence of two distinct behaviors was not appreciated until measurements compared linear substrate to cross-linked ones. Remarkably, the bioelectronic technique allowed the two states to be distinguished, even when they persisted for multiple seconds. The bleaching and blinking of fluorophores makes it very difficult for smFRET to identify inactive periods, much less to separate the two cases as distinct.

A third effect of cross-links was to slightly slow the average rates of lysozyme motions. As shown in Fig. 9d, k_{fast} and k_{slow} decreased by 15% and 20%, respectively, when the linear substrate was replaced with the cross-linked substrate. As noted in Fig. 8, different molecules varied in rate by much more than this amount, but here single molecules were measured processing first one and then the other substrate, a method that allowed direct, comparative measurements. At first glance, it is intuitive that non-hydrolyzable cross-links should slow the average rates of lysozyme activity. The effect on instantaneous rates, on the other hand, is not so clear. Our analysis separated k_{fast} from k_{slow} with single molecule resolution, showing a 20% decrease of k_{slow} that was specific to catalytic hydrolysis. Apparently, cross-links in the substrate slowed the successful catalytic hydrolysis of glycosidic bonds. The cause of this slowing may relate to the cross-linked substrate's increased mechanical stiffness. Furthermore, the cross-links branch off NAM rings, which must also undergo distortion during catalysis; accessing the required skew boat conformation could be more challenging for the cross-linked substrate. Since both linear and cross-linked substrates have identical functional groups close to the site of hydrolysis, such energetic cost must be extracted at some distance from the focus of the enzyme's efforts. This consideration raises the possibility that the cross-links simply interfere with the enzyme's ability to access and grip the relevant NAG–NAM glycosidic bond. Either way, lysozyme's translocation speed along linear portions was slowed when cross-links were present.

Previous smFRET research on lysozyme had suggested that the enzyme was processive,[24] and this data provides the clearest evidence yet. By monitoring a single molecule continuously, we observed continuous catalytic activity for $\langle \tau_{mem} \rangle = 8 \pm 3.0$ s, on average, before any change in rate. At rates of 15 s^{-1}, this duration corresponds to the hydrolysis of 120 $\pm$ 45 glycosidic bonds in succession and without pause. Furthermore, the interruptions of catalytic activity were primarily due to encountering cross-links (blue), as opposed to substrate dissociation (black). When those cross-links were absent, continuous processing for 10 to 30 s without any inactive gaps became typical. Such durations suggest that lysozyme processivity extends to many hundreds of glycosidic bonds, definitively confirming it as a processive enzyme.

In conclusion, the bioelectronic technique for monitoring lysozyme provided a detailed recording of single molecule activity and processivity. We observed molecule-to-molecule variation, but by recording single molecules over long durations we also observed the full range of one molecule's dynamic trajectory.

The technique uncovered 9 independent time constants governing the range of lysozyme's catalytic activity and allowed us to monitor how each one was affected by pH or by substrate cross-links.

Lysozyme variants distinguish the precise transduction mechanism

The previous section focused on the type of electronic data that could be generated by a single lysozyme molecule and conclusions drawn from the analysis of that data. Next, we turn away from the biochemistry of lysozyme to address the electronic transduction at work in these devices. Using lysozyme variants engineered by mutagenesis, we have produced a detailed understanding of the interactions between this enzyme and the SWNT FET. This understanding will help to generalize the bioelectronic technique and make similar signals accessible from a range of proteins.

As described above, SWNTs exhibit exquisite sensitivity to their environment. A single point charge moving near a SWNT is sufficient to change a device's electrical conductance. The doping induced by a point charge is insufficient to cause such a change; instead, the main mechanism responsible for such sensitivity is the electrostatic modulation of other, conductance-limiting barriers. In the case of an attached lysozyme or other protein, for example, the attachment perturbs the SWNT and induces a barrier to conduction. Similar attachments to metal films are well-screened by free carriers, but the ultra-low density of carriers in a SWNT results in very poor screening.[82,83] Consequently, nearby charges can directly influence the barrier and modulate the current flowing through the SWNT. At constant bias, the rapid modulation of this barrier produces the $\Delta I(t)$ fluctuations discussed above.

While this sensitivity leads to good signal transduction, it also results in environmental noise and other variability. For example, absolute conductance values and transconductance sensitivity to gating have proven very difficult to control in SWNTs exposed to their environment.[60,84,85] Even with best fabrication practices, device-to-device variability among SWNTs is widely acknowledged within the field.[86,87] Fortunately for our application with lysozyme, a scheme exists for quantitatively comparing different SWNT devices. This comparison eliminates the device variability that would otherwise preclude molecule-to-molecule comparisons. In fact, we have been able to establish comparisons across dozens of lysozyme-labeled SWNTs, even though the average magnitude of $\Delta I(t)$ fluctuations varied from 20 to 2 nA from one device to another.

Successful device-to-device comparisons required accurate measurements of the characteristic gating dependence of each device. Each SWNT device has a curve $I(V_G)$ that represents the sensitivity of the current to variations in gate voltage V_G. This sensitivity can arise at the metal–SWNT interfaces, from SWNT interactions with the supporting substrate, from the intrinsic SWNT bandstructure, and from the lysozyme attachment itself. Because of this combination of possible factors, all SWNTs exhibit a transconductance dI/dV_G, even when metallic SWNTs are used. The lysozyme attachment acts like a contaminant, perturbing the $I(V_G)$ curve with additional transconductance concentrated at the attachment site.

Fortunately, every lysozyme molecule has identical surface charges and movements. In fact, the exact positions of each residue and its movements are fully determined by X-ray crystallography. Each time a lysozyme is attached to a SWNT, the electric fields from these surface charges have the same sign and magnitude. As the lysozyme undergoes its opening and closing motions, the movement of these charges produces a time-varying electric field that acts in addition to the constant, externally applied V_G to produce a time-varying change in gating ΔV_G. To define this mathematically, consider a set of lysozyme surface charges q_i dynamically varying between positions $x_{i,\mathrm{open}}$ and $x_{i,\mathrm{closed}}$. The consequence of these charges on the SWNT current will be

$$\Delta I \propto \frac{\partial I}{\partial V_G}\sum_i q_i\left(\frac{1}{x_{i,\mathrm{closed}}}-\frac{1}{x_{i,\mathrm{open}}}\right)\exp\left(-x_{i,\mathrm{open}}/\lambda_D\right)=\frac{\partial I}{\partial V_G}\Delta V_G \quad (1)$$

where λ_D is the Debye screening length of the electrolyte.[88] In this equation, the variability of $\Delta I(t)$ from one device to another is entirely due to the slope $\partial I/\partial V_G$, which is an empirical, device-dependent parameter. Otherwise, the q_i and r_i terms in eqn (1) are entirely determined by lysozyme's structure and movements. It is these factors that can be collected into an effective gating term ΔV_G that is device-independent.

Table 2 illustrates the reliability of this comparison for 10 SWNT devices. For each device, the Table lists the initial resistance before bioconjugation, the final resistance with an attached lysozyme, and the transconductance dI/dV_G measured at the operating point $V_G = 0$ V. Each of these three parameters is measured in a buffer electrolyte without peptidoglycan. After adding peptidoglycan, all 10 devices exhibited two-level $\Delta I(t)$ fluctuations with similar timing but magnitudes ranging from 3% to 300%. Using the average ΔI magnitude and the measured transconductance $\partial I/\partial V_G$ around the operating point, an effective gating ΔV_G was calculated for each device. All lysozyme

Table 2 Device characteristics of lysozyme-labeled SWNT FETs

R_{pristine} (MΩ)[a]	$R_{\mathrm{conjugated}}$ (MΩ)[a]	dI/dV_G (%/V)[a]	I_{lo} (nA)[a]	$\langle\Delta I\rangle$ (%)	ΔV_G (V) calc.
Semiconducting SWNTs					
0.28	1.2	95	40	+20	0.21
0.38	1.5	88	103	+18	0.21
0.34	3.0	266	7	+50	0.19
17.6	56	20	2.8	+4	0.20
26.1	40	70	7.2	+14	0.20
Quasi-metallic SWNTs					
0.10	1.4	18	80	+3	0.16
0.30	2.0	46	54	+7	0.15
0.35	2.6	54	45	+10	0.19
1.0	1.8	21	80	+4	0.18
3.0	30	235	3.3	+47	0.20

[a] As measured in buffer electrolyte around the operating point $V_G = 0$ V.

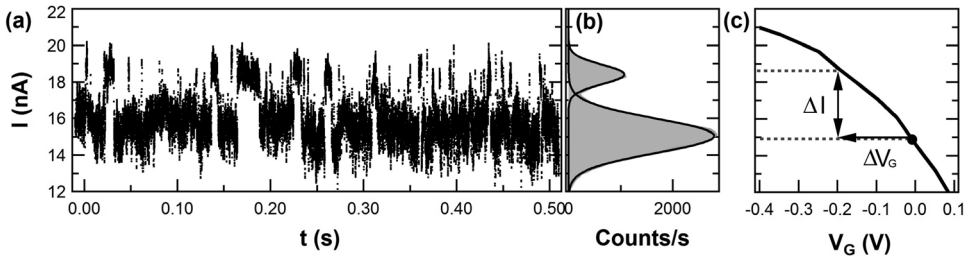

Fig. 10 Calculation of effective gating. Raw $I(t)$ recordings from lysozyme processing (a) can be effectively summarized by a histogram (b) containing separate peaks for the open and closed conformations. (c) The position of the open peak corresponds to the $I(V_G = 0)$ operating point of the device, whereas the position of the closed peak corresponds to a different position on the device's $I(V_G)$ curve. The effective gating of ΔV_G is defined as the change in liquid gate that would produce a ΔI signal of the same magnitude.

devices exhibited $\Delta V_G = -0.19 \pm 0.02$ V, even though some were based upon semiconducting SWNTs and other used metallic SWNTs.

Fig. 10 graphically illustrates the equivalence of describing a particular signal in terms of ΔI or ΔV_G. For a particular $I(t)$ signal, a histogram of the data fit two peaks separated by ΔI. A projection of those peaks onto that device's $I(V_G)$ characteristic shows that the peak of the open conformation is associated with the operating point $V_G = 0$ V (Fig. 10c). The second peak, which in this example is from the transient, closed conformation of lysozyme, suggests a new operating point shifted by the amount ΔV_G. The lysozyme does not actually shift the gate bias felt by the entire SWNT, since the electrolyte environment limits its possible effects to a small region. Nevertheless, treating the ΔI signal as an *effective* shift of gate has proven to be a robust and device-independent way of analyzing the data, as suggested by the formulation of eqn (1).

The applicability of eqn (1) suggested that the primary transduction mechanism was an electrostatic one. To further investigate this effective gating, lysozyme measurements were performed while varying the Debye screening length λ_D of the surrounding buffer. Using an ensemble assay, we initially determined the range of NaCl concentrations in which lysozyme was active, and then single molecule devices were tested under similar conditions. As shown in Fig. 11 for one example device, the $\Delta I(t)$ signal decreased monotonically as the concentration was increased from 50 to 300 mM (in 10 mM phosphate buffer), indicating the increasing effectiveness of electrolyte screening. Other than this decrease in signal amplitude, the overall kinetics and turnover rate of the lysozyme was minimally changed in this range, in accordance with the ensemble measurement.

The screening data were fit to a simple Debye model[89] that determined the relevant distance involved in transduction. Defining x_o as the distance over which the screening is acting, this model predicts a signal amplitude

$$|\Delta I(t)| = A/x_o \exp(-x_o/\lambda_D), \quad (2)$$

where A is a constant of proportionality. Fitting the data in Fig. 11 to eqn (2) produced a value $x_o = 1.03 \pm 0.10$ nm. This distance is remarkably small given that lysozyme is 7 nm tall and that the catalytically active site is located 3.5 nm from the

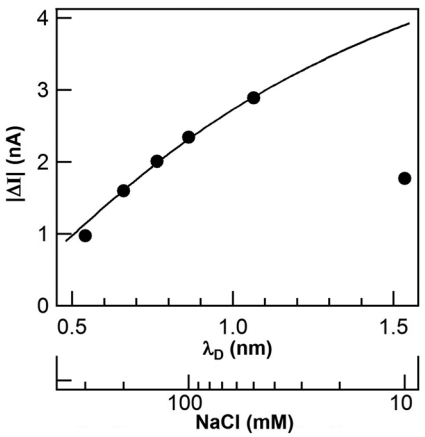

Fig. 11 Effects of electrolyte screening. The average ΔI magnitude generated by a lysozyme increases as the NaCl concentration goes down. The salt concentration is converted to an effective Debye length λ_D on the upper x-axis, and the data are fit to a Debye–Hückel model (solid line). Agreement suggests that the main role of electrolyte is to screen an electrostatic interaction. We believe that the outlier at 10 mM NaCl marks the concentration limit at which lysozyme begins to denature and ultimately become inactive.

SWNT attachment. In fact, such a small x_o indicated that chemical reactions at the far-away active site were definitely not the direct cause of signals in the SWNT. Instead, the response of the SWNT had to result from charges much closer to the attachment site. Similar experiments by others have reached similar conclusions,[68,90,91] with Stern *et al.* using linkers of varying lengths to specifically test that the parameter x_o accurately describes the distance between point charges and a sensitive, nanowire FET.

X-ray crystal structures of lysozyme crystallized in its open and closed conformations allowed us to investigate the possible role of charged surface residues within $\sim x_o$ of the SWNT attachment site. According to the crystal structures (Protein Data Base 1QTV and 148L), only two amino acids were likely candidates for electrostatically gating the SWNT. Sites K83 and R119 were both positively-charged acids, and both moved away from the SWNT upon closure by approximately 0.15 nm.[25,70] No other charged residues near the attachment site moved substantially, and residues further from the attachment site were effectively shielded by the surrounding electrolyte.

Therefore, we focused our attention on the K83 and R119 sidechains, which are highlighted in color in Fig. 3b to depict their motions. The outward motion of these positive charges should result in a weakening of their electric field at the SWNT attachment site, which is consistent with the negative ΔV_G observed experimentally. Therefore, allosteric motions of K83 and R119 had the right properties to provide the necessary link between chemistry at the active site and electrical signal transduction in the SWNT FET.

To experimentally test the role of K83 and R119, we synthesized lysozyme variants with different amino acids at these sites. Using site-directed mutagenesis, the two sites were changed into charge-neutral alanines (K83A and R119A) or negatively-charged glutamic acids (K83E and R119E). With three possible charges at each of two sites, a total of seven distinct lysozyme variants were possible (Fig. 13a). All seven were synthesized, purified, and assayed to check that they had comparable activities. Circular dichroism verified that each variant was properly folded.[15] All seven variants exhibited comparable activities, presumably because neither K83A nor R119A is directly involved in substrate binding or catalytic processing. Finally, each variant was attached to multiple SWNT devices and then monitored under identical conditions hydrolyzing peptidoglycan. Identical fabrication protocols were used without modification, because all of the variants shared the same C90 attachment site. The experiments encompassed over 30 active SWNT devices.

In the presence of substrate, all seven types of devices exhibited dynamic two-level fluctuations ΔI. We immediately observed that the magnitude and sign of ΔI depended on the variant chosen, and categorized each variant by the net charge $N = \sum q_i/e$ of the two residues of interest. Fig. 12 shows example $\Delta I(t)$ signals obtained using two variants. In Fig. 12a, an $N = +1$ variant (R119A) had a signal similar to that discussed previously but approximately half as strong as would be predicted from its $I(V_G)$ curve. In Fig. 12b, an $N = -1$ variant (K83A/R119E) exhibited a signal of similar magnitude but with the opposite sign.

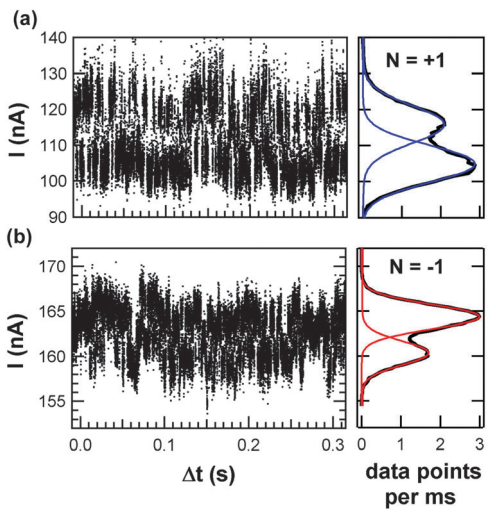

Fig. 12 Example data from of $N = +1$ and $N = -1$ variants. (a) The $N = +1$ variant (R119A) exhibited positive current excursions. (b) The $N = -1$ variant (K83A/R119E) attached to a different SWNT device exhibited negative current excursions. The two signals had similar timing and magnitudes but opposite signs.

To compare dissimilar devices quantitatively, the effective gating ΔV_G from each device was calculated as described above. Fig. 13 summarizes the results by plotting the average ΔV_G for each variant. Error bars in Fig. 13c represent 3 standard deviations.

The $N = 0$ variant (K83A/R119A) produced the smallest fluctuations and had an effective gating of only $\Delta V_G = -34$ mV. This variant was of particular interest because its signal was not generated by charges at sites 83 or 119. Instead, the signal of the $N = 0$ variant was generated by the combined effects of movements by all other lysozyme surface charges and other charge-separated structures (*e.g.*, α-helix dipoles).

Taking this offset $\Delta V_G = -34$ mV to be due to all of the non-targeted amino acids of lysozyme, we could then complete a comparative analysis of signals from variants having charges at sites 83 and/or 119. After being offset by +34 mV, the ΔV_G responses of all seven variants were found to be directly proportional to their net charge N (Fig. 13c, solid squares). The N values of our variants spanned from $N = +2$ to -2, with the initial C90 variant accounting for the highest, $N = 2$ value. The presence of one charged amino acid produced an effective gating of ± 91 mV, and the combined effect of two charged amino acids was approximately twice as large. The response of variants with negative N was equal in magnitude but opposite in sign. Overall, these behaviors exactly match the expectations from the simple electrostatic model of eqn (1), in which ΔV_G is roughly proportional to N. A more detailed analysis of the electrostatics, including tabulated locations and motions of sidechains at sites 83 and 119, was reported in ref. 15. This analysis included an accurate vector calculation of the electric fields from each of the two sites, which indicated that ΔV_G should not quite double when both charges are present but only increase by a factor of 1.85, just as observed experimentally.

Taken together, these results demonstrate the importance of the lysozyme attachment site for producing good signals. Even though lysozyme's distal domain had a net charge of +3 and a substantial hinge motion relative to the C90 attachment site, the effect of its motion was barely 1/3 as large as that from a charge at site 83 or 119. This relatively weak signal is consistent with calculations[92] based solely on the distant domain's net charge and motions. The electrostatic effect of single point charges can be much greater if they are located near the SWNT attachment site (where the SWNT is believed to be most sensitive). For our particular C90 attachment site, two charges located within a screening radius λ_D were found to be responsible for nearly all of the signal observed. Remarkably, even a single charged amino acid was sufficient for producing good signal-to-noise (Fig. 12). Four separate variants with single point charges (*i.e.* $|N| = 1$) were tested experimentally. All four were similarly effective at signal generation, producing signals with a sensitivity $|\Delta V_G| = 91$ mV that was nearly three times

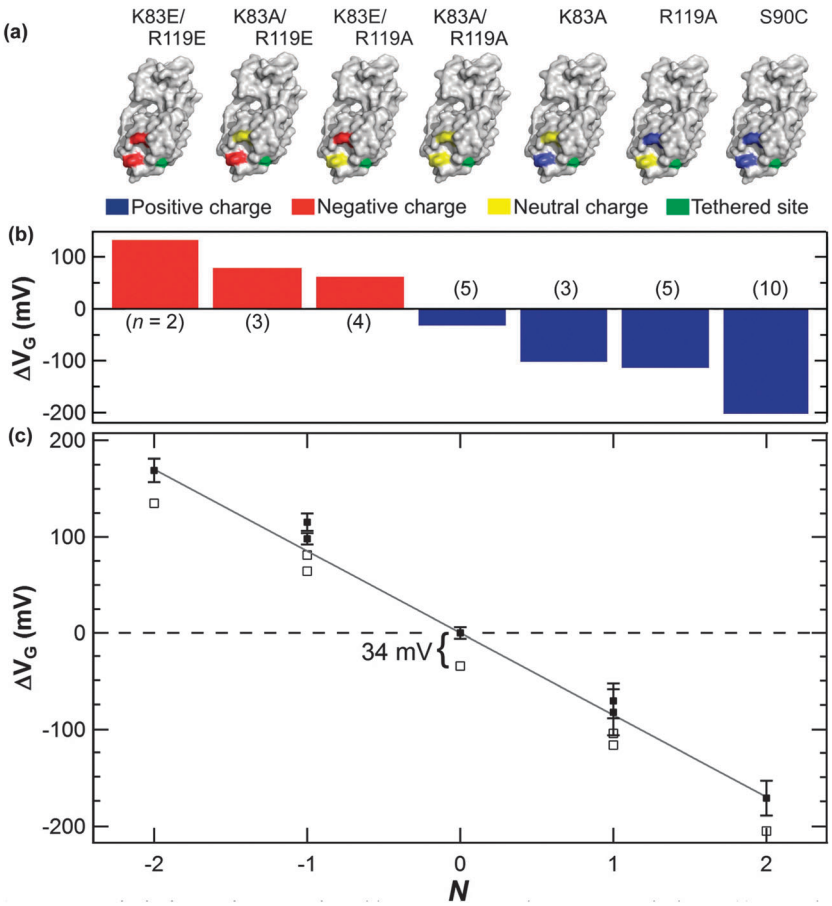

Fig. 13 Average transduction by seven lysozyme variants. (a) Lysozyme sites 83 and 119 were mutated to have positive, neutral, or negative charged sidechains. (b) The average effective gating ΔV_G as determined from n different devices fabricated with each variant. ΔV_G varied from 135 to −205 mV, with a value of −34 mV for the neutral $N = 0$ variant. (c) For all seven variants, ΔV_G was proportional to N (fit shown with solid line, $R^2 = 0.992$), with a slope of −87 ± 2 mV per unit charge. Raw data are shown as open squares. Shifting the data up by 34 mV to account for the neutral variant (solid squares) results in a response that is symmetric around zero. Error bars indicate three standard deviations.

greater than the effect of all the other surface charges and their motions.

Thus, the design of the attachment site is probably critical to successful transduction. The presence of one or more charged groups moving together near the attachment site is the main predictor of a good signal strength. The measurements here prove that the immediate electrostatic environment of the attachment site is most important for transduction. This result is contrary to predictions that an effective attachment site would need to be located near the enzyme's active sites for binding or catalysis. In fact, attachments at those positions can interfere with activity and perturb kinetics, which is always an issue when fluorophores are incorporated for smFRET measurements. Another aspect of attachment bearing consideration is that the C90 site used here was relatively rigid with respect to the enzyme's center of mass. Opening and closing motions of the enzyme could occur without unnecessary deformation of the SWNT–lysozyme linkage. We speculate that similarly immobile sites might also be an important criteria for optimizing SWNT attachment sites.

Compared to the issues of choosing the right position for protein attachment and good transduction, the particular properties of the SWNT device were relatively inconsequential. Devices formed from metallic SWNTs performed just as well as ones with semiconducting SWNTs, and variability of contact resistance to the SWNT was not an issue in the measurements. The signal-to-noise ratio of a single molecule recording was not substantially improved by selecting the steeper $I(V_G)$ curves of semiconducting SWNTs, because that same enhancement of sensitivity led to higher background noise. In practice, we found that most of our devices were suitable for lysozyme labeling and monitoring, indicating that the techniques used here could be scaled up to the production of many devices in parallel. In fact, the main barrier to most SWNT electronic applications—namely, the chiral variability of SWNTs that produces mixtures of semiconducting and metallic species—did not limit their use here as single molecule sensors. The single device criterion that did matter, in our experience, was avoiding as-fabricated devices that exhibited high noise or two-level switching. Because the lysozyme activity was encoded as an electronic fluctuation, devices with pre-existing fluctuations from defects, contaminants, and active traps in the underlying oxide were unsuitable for measurement.

Opportunities for electronic single molecule enzymology

The previous section has addressed the design rules necessary to predict the success and applicability of lysozyme-based single molecule devices. Experiments proved that a simple, electrostatic gating mechanism was responsible for signal transduction in the SWNT FET. Mechanical displacements of charged functionalities were the primary sources of transduction, and by selecting or creating these functionalities the signal strength was optimized.

While this work was conducted with T4 lysozyme, the results are general and suggest that other enzymes could be studied equally well. The key information for predicting the success or failure of a particular lysozyme variant was the allosteric movements of charged residues near a desired attachment site. Designing effective devices, therefore, should be possible for any other enzyme, as long as good X-ray crystal structure data exist for the conformational states of interest. By comparing the motions of individual amino acids, an attachment site can be selected or surface residues can be modified to help generate strong electronic signals. Furthermore, single-residue sensitivity has been demonstrated with lysozyme, indicating that the electronic technique only requires minimal modifications to the enzyme of interest, if any.

This design strategy is unlikely to be unique to lysozyme. In fact, ongoing research using the techniques described above is already proving successful in our laboratory for two enzymes unrelated to lysozyme. In one case, a ternary complex between an enzyme, its substrate, and a co-factor has led to three distinct conformations, and these three conformations have produced three unique $I(t)$ levels in SWNT devices.[16] In another case, an enzyme that can process many possible substrates has been studied to find that each substrate generates an electronic signal with different kinetics and other attributes.[17] While these initial results extend far beyond the topic of this review, they support the conclusion that the electronic platform can be generalized.

As a limitation of this rule, we note that past lysozyme research provided substantial guidance to the interpretation of the electronic recordings described here. Lysozyme had been well studied by ensemble assays,[93,94] X-ray crystal structures,[58,69] NMR dynamics,[95,96] and single molecule techniques like smFRET,[24,26,27,77] and all of these contributed substantially to our interpretation of the electronic data. Without a foreknowledge of lysozyme's memory effects and the presence of both fast and slow switching, our progress understanding complex $I(t)$ signals from lysozyme would have proceeded much more slowly. While the electronic recordings provided rich details about lysozyme's activity, they might have been indecipherable in isolation. Research on other enzymes might produce similarly complex electronic signals, which will only be meaningful when interpreted within a context of more traditional single molecule and ensemble techniques.

Nevertheless, once a framework for interpreting the data has been built, the electronic recordings contain types of information that are inaccessible to most other techniques. At fast time scales, the temporal resolution of the electronic signal far surpasses fluorescence-based techniques. Without any device optimization, resolutions of 20 μs were immediately obtained, and there are no fundamental reasons that the SWNT device response cannot be pushed well below 1 μs to directly observe details of transitions and intermediate states. At that scale, the SWNT technique begins to overlap and complement dynamic data obtained using NMR. At the other end of the time scale, the stability of the electronic technique allows monitoring of the same molecule over minutes to hours, even as it is probed in different solutions or at different temperatures. This attribute allowed us to directly observe the effects of pH on some, but certainly not all, of the parameters governing lysozyme productivity. Continuous long-term monitoring promises to distinguish between ''static'' disorder and ''dynamic'' disorder in the time range of minutes and hours, where transitions between metastable conformations can be very slow.

Furthermore, because the electronic method is label-free and not optical, it constitutes a readout channel of molecular function that is truly independent of fluorescence-based single-molecule techniques. By combining electronic recording with FRET labels on either the protein or substrate, simultaneous optical and electronic readout of a single molecule becomes possible, at least in principle. The electronic and optical techniques are transduced by two different mechanisms from two distinct portions of the same molecule, providing a powerful combination for new studies. The opportunity to establish the relative ordering and delay between events like charge transfer and conformational change, for example, requires two, independent readouts like that described here.

Finally, preliminary success monitoring lysozyme suggests a wide range of practical uses for single molecule bioelectronics. Besides the reaction of enzymes with substrates, there are opportunities to study the effects of cofactors or to screen for inhibitors. Enzyme assays for inhibitor discovery typically require the synthesis of substantial quantities of each potential inhibitor. The ability to work at the single molecule scale allows the same active site of a given molecule to be screened against a library of possible inhibitors, all with minimal reagent usage. Alternatively, nanocircuits could be fabricated using proteins having mutations suspected of being implicated in diseases. Such devices could simplify pharmaceutical searches for molecules that inhibit one class of variant but not another. In fact, the biomolecule nanocircuit technique could emerge as a cost- and time-saving solution to traditional chemical synthesis and purification. In this manner, single-molecule electronic enzymology could accelerate drug discovery through early stage, information-rich screening.

Conclusion

In conclusion, we have demonstrated that lysozyme motions can electrostatically transduce electronic signals in an underlying SWNT FET and that a single amino acid, when properly located, is sufficient to generate useful signals.

The resulting dynamic signals provided a detailed, bond-by-bond recording of lysozyme's activity, allowing us to elucidate key aspects of its catalytic activity. We immediately distinguished lysozyme's fast, nonproductive motions from its slow catalytic processing, and using long-duration recordings observed interconversion rates between the two types of activity as slow as 0.05 s^{-1}. At least nine independent time constants were necessary to fully describe lysozyme's activity, and each of these parameters were studied as a function of pH. The pH did not change lysozyme's instantaneous kinetics, but had its main effect by dramatically increasing the proportion of time spent in nonproductive or inactive states. Using a synthetic, linear substrate, we also determined the effects of cross-links on these time constants, observing that cross-links also trap the enzyme in its nonproductive state. The statistical analysis of many thousands of events determined that lysozyme closes with a single rate-limiting step but opens in a multi-step process, even when in a nonproductive sequence involving no chemical modification. The recordings identified lysozyme as a processive enzyme able to cleave hundreds of glycosidic bonds when not interrupted by cross-links.

Uncovering such a wide range of new information for an enzyme that had been studied for over a century suggests that the single molecule bioelectronic technique holds great promise. Generalization of the bioelectronic technique is possible because of the design rules described here. The fact that our strategies have been successfully applied to two additional enzymes besides lysozyme indicates that similar dynamic signals might be generated from an unlimited number of proteins. If so, then single molecule bioelectronics could have substantial impacts on enzymology and its related fields, especially when used in combination with other traditional techniques.

Acknowledgements

The work described here was made possible by the contributions of many talented students and postdocs, and by financial support from the National Science Foundation (DMR-0801271, DMR-1104629, and ECCS-1231910) and the National Cancer Institute of the NIH (R01 CA133592-01).

Notes and references

1 C. Acevedo-Vélez, G. Andre, Y. F. Dufrêne, S. H. Gellman and N. L. Abbott, *J. Am. Chem. Soc.*, 2011, **133**, 3981–3988.
2 A. B. Churnside, R. M. A. Sullan, D. M. Nguyen, S. O. Case, M. S. Bull, G. M. King and T. T. Perkins, *Nano Lett.*, 2012, **12**, 3557–3561.
3 R. Zhu, S. Howorka, J. Proll, F. Kienberger, J. Preiner, J. Hesse, A. Ebner, V. P. Pastushenko, H. J. Gruber and P. Hinterdorfer, *Nat. Nanotechnol.*, 2010, **5**, 788–791.
4 R. Liu, S. Garcia-Manyes, A. Sarkar, C. L. Badilla and J. M. Fernández, *Biophys. J.*, 2009, **96**, 3810–3821.
5 A. P. Wiita, R. Perez-Jimenez, K. A. Walther, F. Grater, B. J. Berne, A. Holmgren, J. M. Sanchez-Ruiz and J. M. Fernandez, *Nature*, 2007, **450**, 124–127.
6 K. L. Frieda and S. M. Block, *Science*, 2012, **338**, 397–400.
7 D. H. Paik and T. T. Perkins, *Angew. Chem., Int. Ed.*, 2012, **51**, 1811–1815.
8 K. C. Neuman and A. Nagy, *Nat. Methods*, 2008, **5**, 491–505.
9 W. E. Moerner and L. Kador, *Phys. Rev. Lett.*, 1989, **62**, 2535–2538.
10 S. N. Xie, *Single Mol.*, 2001, **2**, 229–236.
11 W. Min, B. English, G. Luo, B. Cherayil, S. Kou and X. Xie, *Acc. Chem. Res.*, 2005, **38**, 923–931.
12 J. Hohlbein, K. Gryte, M. Heilemann and A. N. Kapanidis, *Phys. Biol*, 2010, **7**, 031001.
13 Y. Choi, I. S. Moody, P. C. Sims, S. R. Hunt, B. L. Corso, D. E. Seitz, L. C. Blaszcazk, P. G. Collins and G. A. Weiss, *J. Am. Chem. Soc.*, 2012, **134**, 2032–2035.
14 Y. Choi, I. S. Moody, P. C. Sims, S. R. Hunt, B. L. Corso, G. A. Weiss and P. G. Collins, *Science*, 2012, **335**, 319–324.
15 Y. Choi, T. J. Olsen, P. C. Sims, I. S. Moody, B. L. Corso, M. N. Dang, G. A. Weiss and P. G. Collins, *Nano Lett.*, 2013, **13**, 625–631.
16 P. C. Sims, I. S. Moody, Y. Choi, C. Dong, M. Iftikhar, B. L. Corso, O. T. Gul, P. G. Collins and G. A. Weiss, *J. Am. Chem. Soc.*, 2013, **135**, 7861–7868.
17 T. J. Olsen, Y. Choi, P. C. Sims, O. T. Gul, B. L. Corso, C. Dong, W. A. Brown, P. G. Collins and G. A. Weiss, *J. Am. Chem. Soc.*, 2013, **135**, 7855–7860.
18 S. O. Meroueh, K. Z. Bencze, D. Hesek, M. Lee, J. F. Fisher, T. L. Stemmler and S. Mobashery, *Proc. Natl. Acad. Sci. U. S. A.*, 2006, **103**, 4404–4409.
19 R. H. Jacobson, M. Matsumura, H. R. Faber and B. W. Matthews, *Protein Sci.*, 1992, **1**, 46–57.
20 M. Delepierre, C. M. Dobson, M. Karplus, F. M. Poulsen, D. J. States and R. E. Wedin, *J. Mol. Biol.*, 1987, **197**, 111–122.
21 C. B. Post, B. R. Brooks, M. Karplus, C. M. Dobson, P. J. Artymiuk, J. C. Cheetham and D. C. Phillips, *J. Mol. Biol.*, 1986, **190**, 455–479.
22 C. C. F. Blake, D. F. Koenig, G. A. Mair, A. C. T. North, D. C. Phillips and V. R. Sarma, *Nature*, 1965, **206**, 757–761.
23 H. R. Faber and B. W. Matthews, *Nature*, 1990, **348**, 263–266.
24 D. Hu and H. P. Lu, *Biophys. J.*, 2004, **87**, 656–661.
25 R. Kuroki, L. H. Weaver and B. W. Matthews, *Proc. Natl. Acad. Sci. U. S. A.*, 1999, **96**, 8949–8954.
26 Y. Chen, D. H. Hu, E. R. Vorpagel and H. P. Lu, *J. Phys. Chem. B*, 2003, **107**, 7947–7956.
27 Y. Wang and H. P. Lu, *J. Phys. Chem. B*, 2010, **114**, 6669–6674.
28 R. Kuroki, L. H. Weaver and B. W. Matthews, *Nat. Struct. Biol.*, 1995, **2**, 1007–1011.
29 H. S. McHaourab, K. J. Oh, C. J. Fang and W. L. Hubbell, *Biochemistry*, 1997, **36**, 307–316.
30 R. Q. Zhou, S. G. Chen and P. Recsei, *Anal. Biochem.*, 1988, **171**, 141–144.
31 C. P. Collier, E. W. Wong, M. Belohradsky, F. M. Raymo, J. F. Stoddart, P. J. Kuekes, R. S. Williams and J. R. Heath, *Science*, 1999, **285**, 391.
32 T. I. Kamins and R. S. Williams, *MST News Pol.*, 2001, 34–36.
33 N. A. Melosh, A. Boukai, F. Diana, B. Gerardot, A. Badolato, P. M. Petroff and J. R. Heath, *Science*, 2003, **300**, 112–115.

34 F. Patolsky, G. F. Zheng and C. M. Lieber, *Anal. Chem.*, 2006, **78**, 4260–4269.
35 M. A. Reed, C. Zhou, C. J. Muller, T. P. Burgin and J. M. Tour, *Science*, 1997, **278**, 252–254.
36 J. Chen, M. A. Reed, A. M. Rawlett and J. M. Tour, *Science*, 1999, **286**, 1559.
37 M. T. Gonzalez, S. M. Wu, R. Huber, S. J. van der Molen, C. Schonenberger and M. Calame, *Nano Lett.*, 2006, **6**, 2238–2242.
38 N. J. Tao, *J. Mater. Chem.*, 2005, **15**, 3260–3263.
39 L. Venkataraman, Y. S. Park, A. C. Whalley, C. Nuckolls, M. S. Hybertsen and M. L. Steigerwald, *Nano Lett.*, 2007, **7**, 502–506.
40 H. Park, A. K. L. Lim, A. P. Alivisatos, J. Park and P. L. McEuen, *Appl. Phys. Lett.*, 1999, **75**, 301–303.
41 Y. Lu, B. Goldsmith, D. R. Strachan, J. H. Lim, Z. T. Luo and A. T. C. Johnson, *Small*, 2010, **6**, 2748–2754.
42 D. R. Strachan, D. E. Smith, D. E. Johnston, T. H. Park, M. J. Therien, D. A. Bonnell and A. T. Johnson, *Appl. Phys. Lett.*, 2005, **86**, 43109.
43 R. Sordan, K. Balasubramanian, M. Burghard and K. Kern, *Appl. Phys. Lett.*, 2005, **87**, 013106.
44 A. Star, J. C. P. Gabriel, K. Bradley and G. Gruner, *Nano Lett.*, 2003, **3**, 459–463.
45 A. Star, T. R. Han, V. Joshi, J. C. P. Gabriel and G. Gruner, *Adv. Mater.*, 2004, **16**, 2049–2052.
46 K. Besteman, J. O. Lee, F. G. M. Wiertz, H. A. Heering and C. Dekker, *Nano Lett.*, 2003, **3**, 727–730.
47 G. Gruner, *Anal. Bioanal. Chem.*, 2006, **384**, 322–335.
48 X. Guo, J. P. Small, J. E. Klare, Y. Want, M. S. Purewal, I. W. Tam, B. H. Hong, R. Caldwell, L. Huang, S. O'Brien, J. Yan, R. Breslow, S. J. Wind, J. Hone, P. Kim and C. Nuckolls, *Science*, 2006, **311**, 356–359.
49 S. Liu, X. Zhang, W. Luo, Z. Wang, X. Guo, M. L. Steigerwald and X. Fang, *Angew. Chem., Int. Ed.*, 2011, **50**, 2496–2502.
50 Y. Cui, Q. Q. Wei, H. K. Park and C. M. Lieber, *Science*, 2001, **293**, 1289–1292.
51 F. Patolsky, G. Zheng, O. Hayden, M. Lakadamyali, X. Zhuang and C. M. Lieber, *Proc. Natl. Acad. Sci. U. S. A.*, 2004, **101**, 14017–14022.
52 G. F. Zheng, F. Patolsky, Y. Cui, W. U. Wang and C. M. Lieber, *Nat. Biotechnol.*, 2005, **23**, 1294–1301.
53 Z. Li, B. Rajendran, T. I. Kamins, X. Li, Y. Chen and R. S. Williams, *Appl. Phys. A: Mater. Sci. Process.*, 2005, **80**, 1257–1263.
54 F. Patolsky, B. P. Timko, G. H. Yu, Y. Fang, A. B. Greytak, G. F. Zheng and C. M. Lieber, *Science*, 2006, **313**, 1100–1104.
55 Y. Fang, F. Patolsky and C. M. Lieber, *Biophys. J.*, 2007, 551A.
56 S. J. Park, T. A. Taton and C. A. Mirkin, *Science*, 2002, **295**, 1503–1506.
57 Y. Xiao, F. Patolsky, E. Katz, J. F. Hainfeld and I. Willner, *Science*, 2003, **299**, 1877–1881.
58 F. Schedin, A. K. Geim, S. V. Morozov, E. W. Hill, P. Blake, M. I. Katsnelson and K. S. Novoselov, *Nat. Mater.*, 2007, **6**, 652–655.
59 Y. Lu, B. R. Goldsmith, N. J. Kybert and A. T. C. Johnson, *Appl. Phys. Lett.*, 2010, **97**, 083107.
60 P. G. Collins, K. Bradley, M. Ishigami and A. Zettl, *Science*, 2000, **287**, 1801–1804.
61 J. Kong, N. R. Franklin, C. W. Zhou, M. G. Chapline, S. Peng, K. J. Cho and H. J. Dai, *Science*, 2000, **287**, 622–625.
62 K.-J. Lee and J. Kong, in *Carbon Nanotube Electronics*, ed. A. Javey and J. Kong, Springer, New York, 2009.
63 B. R. Goldsmith, J. G. Coroneus, V. R. Khalap, A. A. Kane, G. A. Weiss and P. G. Collins, *Science*, 2007, **315**, 77–81.
64 J. G. Coroneus, B. R. Goldsmith, J. A. Lamboy, A. A. Kane, P. G. Collins and G. A. Weiss, *ChemPhysChem*, 2008, **9**, 1053–1056.
65 B. R. Goldsmith, J. G. Coroneus, A. A. Kane, G. A. Weiss and P. G. Collins, *Nano Lett.*, 2008, **8**, 189–194.
66 B. R. Goldsmith, J. G. Coroneus, J. Lamboy, G. A. Weiss and P. G. Collins, *J. Mater. Res.*, 2008, **23**, 1197–1201.
67 S. Sorgenfrei, C.-y. Chiu, R. L. Gonzalez, Y.-J. Yu, P. Kim, C. Nuckolls and K. L. Shepard, *Nat. Nanotechnol.*, 2011, **6**, 126–132.
68 S. Sorgenfrei, C.-y. Chiu, M. Johnston, C. Nuckolls and K. L. Shepard, *Nano Lett.*, 2011, **11**, 3739–3743.
69 R. J. Chen, Y. G. Zhan, D. W. Wang and H. J. Dai, *J. Am. Chem. Soc.*, 2001, **123**, 3838–3839.
70 R. Kuroki, L. H. Weaver and B. W. Matthews, *Science*, 1993, **262**, 2030–2033.
71 G. T. Hermanson, *Bioconjugate Techniques*, Academic Press, Inc., Chicago, 2008.
72 S. Johnson and S. Cain, *Appl. Opt.*, 2008, **47**, 5147–5154.
73 R. J. Chen, S. Bangsaruntip, K. A. Drouvalakis, N. W. S. Kam, M. Shim, Y. M. Li, W. Kim, P. J. Utz and H. J. Dai, *Proc. Natl. Acad. Sci. U. S. A.*, 2003, **100**, 4984–4989.
74 R. J. Chen, H. C. Choi, S. Bangsaruntip, E. Yenilmez, X. Tang, Q. Wang, Y.-L. Chang and H. Dai, *J. Am. Chem. Soc.*, 2004, **126**, 1563–1568.
75 P. G. Collins, M. S. Fuhrer and A. Zettl, *Appl. Phys. Lett.*, 2000, **76**, 894–896.
76 Y.-M. Lin, J. Appenzeller, J. Knoch, Z. Chen and P. Avouris, *Nano Lett.*, 2006, **6**, 930–936.
77 H. P. Lu, *Curr. Pharm. Biotechnol.*, 2004, **5**, 261–269.
78 K. Svoboda, P. P. Mitra and S. M. Block, *Proc. Natl. Acad. Sci. U. S. A.*, 1994, **91**, 11782–11786.
79 M. J. Schnitzer and S. M. Block, *Cold Spring Harbor Symp. Quant. Biol.*, 1995, **60**, 793–802.
80 W. L. Xu, J. S. Kong and P. Chen, *J. Phys. Chem. C*, 2009, **113**, 2393–2404.
81 M. S. VanNieuwenhze, S. C. Mauldin, M. Zia-Ebrahimi, B. E. Winger, W. J. Hornback, S. L. Saha, J. A. Aikins and L. C. Blaszczak, *J. Am. Chem. Soc.*, 2002, **124**, 3656.
82 F. Leonard and J. Tersoff, *Phys. Rev. Lett.*, 1999, **83**, 5174–5177.
83 F. Leonard and A. A. Talin, *Nat. Nanotechnol.*, 2011, **6**, 773–783.
84 M. Kruger, I. Widmer, T. Nussbaumer, M. Buitelaar and C. Schonenberger, *New J. Phys.*, 2003, **5**, 138.

85 X. Y. Sun and Y. G. Sun, *J. Mater. Sci. Technol.*, 2008, **24**, 569–577.
86 Z. Chen, J. Appenzeller, J. Knoch, Y. Lim and P. Avouris, *Nano Lett.*, 2005, **5**, 1497.
87 A. D. Franklin, G. S. Tulevski, S.-J. Han, D. Shahrjerdi, Q. Cao, H.-Y. Chen, H. S. P. Wong and W. Haensch, *ACS Nano*, 2012, **6**, 1109–1115.
88 J. N. Israelachvili, *Intermolecular and surface forces*, Academic Press, London, 1991.
89 P. Debye and E. Huckel, *Phys. Z.*, 1923, **24**, 185–206.
90 I. Heller, S. Chatoor, J. Mannik, M. A. G. Zevenbergen, C. Dekker and S. G. Lemay, *J. Am. Chem. Soc.*, 2010, **132**, 17149–17156.
91 E. Stern, R. Wagner, F. J. Sigworth, R. Breaker, T. M. Fahmy and M. A. Reed, *Nano Lett.*, 2007, **7**, 3405–3409.
92 L. Prisbrey, G. Schneider and E. Minot, *J. Phys. Chem. B*, 2010, **114**, 3330–3333.
93 H. B. Jensen and K. Kleppe, *Eur. J. Biochem.*, 1972, **28**, 116–122.
94 W. A. Baase, L. Liu, D. E. Tronrud and B. W. Matthews, *Protein Sci.*, 2010, **19**, 631–641.
95 F. A. A. Mulder, N. R. Skrynnikov, B. Hon, F. W. Dahlquist and L. E. Kay, *J. Am. Chem. Soc.*, 2001, **123**, 967–975.
96 L. P. McIntosh, R. H. Griffey, D. C. Muchmore, C. P. Nielson, A. G. Redfield and F. W. Dahlquist, *Proc. Natl. Acad. Sci. U. S. A.*, 1987, **84**, 1244–1248.